AFRL-ML-WP-TP-2003-415

CHARACTERIZATION OF FRETTING FATIGUE CRACK INITIATION PROCESSES IN CR Ti-6A1-4V

A. L. Hutson
C. Neslen
T. Nicholas

FEBRUARY 2003

Approved for public release; distribution is unlimited.

MATERIALS AND MANUFACTURING DIRECTORATE
AIR FORCE RESEARCH LABORATORY
AIR FORCE MATERIEL COMMAND
WRIGHT-PATTERSON AIR FORCE BASE, OH 45433-7750

REPORT DOCUMENTATION PAGE

Form Approved
OMB No. 0704-0188

1. REPORT DATE *(DD-MM-YY)*	2. REPORT TYPE	3. DATES COVERED *(From - To)*
February 2003	Journal Article	

4. TITLE AND SUBTITLE
CHARACTERIZATION OF FRETTING FATIGUE CRACK INITIATION PROCESSES IN CR Ti-6A1-4V

5a. CONTRACT NUMBER
F33615-98-C-5214

5b. GRANT NUMBER

5c. PROGRAM ELEMENT NUMBER
62102F

6. AUTHOR(S)
A. L. Hutson
C. Neslen
T. Nicholas

5d. PROJECT NUMBER
4347

5e. TASK NUMBER
52

5f. WORK UNIT NUMBER
01

7. PERFORMING ORGANIZATION NAME(S) AND ADDRESS(ES)
Plans and Programs Branch (AFRL/MLOP)
Integration and Operations Division
Materials and Manufacturing Directorate
Air Force Research Laboratory, Air Force Materiel Command
Wright-Patterson AFB, OH 45433-7750

8. PERFORMING ORGANIZATION REPORT NUMBER

9. SPONSORING/MONITORING AGENCY NAME(S) AND ADDRESS(ES)
Materials and Manufacturing Directorate
Air Force Research Laboratory
Air Force Materiel Command
Wright-Patterson AFB, OH 45433-7750

10. SPONSORING/MONITORING AGENCY ACRONYM(S)
AFRL/MLOP

11. SPONSORING/MONITORING AGENCY REPORT NUMBER(S)
AFRL-ML-WP-TP-2003-415

12. DISTRIBUTION/AVAILABILITY STATEMENT
Approved for public release; distribution is unlimited.

13. SUPPLEMENTARY NOTES

Published in *Tribology International*, Vol: 36, Issue: 2, pp. 133-143, February 2003.

14. ABSTRACT
A study was conducted to quantify fretting fatigue damage and to evaluate the residual fatigue strength of specimens subjected to a range of fretting fatigue test conditions. Flat Ti-6A1-4V specimen were tested against flat Ti-6A1-4V fretting pads with blending radii at the edges of contact. Fretting fatigue damage for two combinations of static average clamping stress and applied axial stress was investigated for two percentages of total life. Accumulated damage was characterized using full field surface roughness evaluation and scanning electron microscopy (SEM). The effect of fretting fatigue on uniaxial fatigue strength was quantified by interrupting fretting fatigue tests, and conducting uniaxial residual fatigue strength tests at R = 0.5 at 300 Hz. Results from the residual fatigue strength tests were correlated with characterization results.

15. SUBJECT TERMS
Fretting fatigue; Ti-6Al-4V; Surface roughness

16. SECURITY CLASSIFICATION OF:			17. LIMITATION OF ABSTRACT:	18. NUMBER OF PAGES	19a. NAME OF RESPONSIBLE PERSON (Monitor)
a. REPORT	b. ABSTRACT	c. THIS PAGE			Craig Neslen
Unclassified	Unclassified	Unclassified	SAR	18	19b. TELEPHONE NUMBER *(Include Area Code)* (937) 656-9213

HES&S 31-15093-1

Standard Form 298 (Rev. 8-98)
Prescribed by ANSI Std. Z39-18

ELSEVIER

Tribology International 36 (2003) 133–143

TRIBOLOGY INTERNATIONAL

www.elsevier.com/locate/triboint

Characterization of fretting fatigue crack initiation processes in CR Ti–6Al–4V

A.L. Hutson [a,*], C. Neslen [b], T. Nicholas [b]

[a] *University of Dayton Research Institute, 300 College Park, Dayton, OH 45469-0128, USA*

[b] *Air Force Research Laboratory, Materials and Manufacturing Directorate, Wright–Patterson Air Force Base, OH 45433, USA*

Abstract

A study was conducted to quantify fretting fatigue damage and to evaluate the residual fatigue strength of specimens subjected to a range of fretting fatigue test conditions. Flat Ti–6Al–4V specimens were tested against flat Ti–6Al–4V fretting pads with blending radii at the edges of contact. Fretting fatigue damage for two combinations of static average clamping stress and applied axial stress was investigated for two percentages of total life. Accumulated damage was characterized using full field surface roughness evaluation and scanning electron microscopy (SEM). The effect of fretting fatigue on uniaxial fatigue strength was quantified by interrupting fretting fatigue tests, and conducting uniaxial residual fatigue strength tests at $R = 0.5$ at 300 Hz. Results from the residual fatigue strength tests were correlated with characterization results.

While surface roughness measurements, evaluated in terms of asperity height and asperity spacing, reflected changes in the specimen surfaces as a result of fretting fatigue cycling, those changes did not correspond to decreases in residual fatigue strength. Neither means of evaluating surface roughness was able to identify cracks observed during SEM characterization. Residual fatigue strength decreased only in the presence of fretting fatigue cracks with surface lengths of 150 μm or greater, regardless of contact condition or number of applied fretting fatigue cycles. No cracks were observed on specimens tested at the lower stress condition. Threshold stress intensity factors were calculated for cracks identified during SEM characterization. The resulting values were consistent with the threshold identified for naturally initiated cracks that were stress relieved to remove load history effects. Published by Elsevier Science Ltd.

Keywords: Fretting fatigue; Ti–6Al–4V; Surface roughness

1. Introduction

In 1912, Eden et al. documented findings on a newly discovered phenomenon they identified as fretting corrosion [1]. That paper is considered the first acknowledgement of damage occurring due to the presence of contact between components, and so marks the commencement of study of the effect of contact on structural components. Since that landmark publication, research has been undertaken worldwide to characterize and describe the effects of contact and to understand the sources and progression of contact-related damage [2,3]. During this time, different regimes, characterized mainly by the magnitude of displacement between the components, have been identified experimentally. These regimes, identified as gross slip (fretting wear or galling), mixed slip–stick (fretting fatigue), and stick, have been associated with different damage mechanisms, namely, wear (material removal), cracking and 'no damage', of which cracking is considered the most detrimental [4,5].

Identifying these regimes in service components is an extremely difficult task that is not, as yet, totally resolved. In service, the regimes may overlap, causing damage from one regime to be obscured by another—and the transition from one regime to another is unclear, causing further confusion. Thus, the result has been efforts to identify detrimental surface conditions resulting from the contact using criteria whose validity is yet to be proven.

Currently, ultrasonic crack detection and surface features are used to identify fretted components for retirement in the aircraft industry. Existing ultrasonic crack

* Corresponding author. Tel.: +1-937-255-2708; fax: +1-937-255-1363.

E-mail address: alisha.hutson@wpafb.af.mil (A.L. Hutson).

0301-679X/03/$ - see front matter Published by Elsevier Science Ltd.
PII: S0301-679X(02)00138-X

detection technology is hampered by the presence of fretting fatigue roughened surfaces, which may themselves indicate underlying component damage, particularly for blade disk attachments in turbine engines. While this criterion is widely accepted and used to retire costly components, almost no research has been conducted to verify it.

Some efforts have been made to quantify surface features for fretting fatigue [6–9]. The United States Air Force has sponsored work to document surface roughnesses of retired engine components, although no efforts have yet been made to determine the remaining life of those components [10]. The effects of surface roughness on predicted stress profiles have been used to predict fatigue lives of laboratory specimens [8]. Shell and Eylon reported a technique to quantify surface roughnesses of fretted laboratory specimens [9]. The technique was capable of distinguishing between slip, stick and non-contacted regions on those specimens, but the results were never related to underlying damage.

The work discussed in this paper attempts to correlate the surface features quantified using the technique reported by Shell and Eylon with residual fatigue strength of Ti–6Al–4V laboratory specimens. A novel test geometry that simulates the essential loading and geometry features of a turbine engine blade root attachment while maintaining the simplicity of a more generalized geometry is employed [11,12]. Normal and shear loads similar to those present in the dovetail blade attachment during steady state operation are applied to the specimen, as shown in Fig. 1. The bending moment indicated on the specimen has been shown to be relatively small and may be neglected [13]. This apparatus also produces the same type of damage as one of the types investigated in the work by Shell and Eylon.

2. Experimental approach

Two objectives were defined for the current investigation: quantify the reduction of fatigue strength caused by fretting fatigue damage accumulated at two levels of fretting fatigue life, and verify the viability of surface roughness to quantify fretting fatigue damage. To achieve these objectives two series of tests were conducted: one in which the fretting fatigue portion of the experiment was interrupted at a predetermined portion of fretting fatigue life (referred to as 10%-of-life tests), and the other in which the specimen was tested until fracture (referred to as 100%-of-life tests). Details on how these tests were conducted are discussed below. These tests were conducted for two combinations of axial and clamping stress. Each series of tests involved application of fretting fatigue cycles, followed by characterization of the fretting damage, heat-tinting to mark the size and location of fretting fatigue-generated cracks, and finally fracture of each specimen under uniaxial fatigue cycling.

2.1. Material and machining parameters

Fretting fatigue specimens and pads were machined from forged Ti–6Al–4V plates with an $\alpha + \beta$ duplex microstructure. Axial specimens were machined with the fatigue axis oriented in the longitudinal direction. Orientation of the pads was not specified or identified. The material yield strength is 930 MPa; the tensile strength is 980 MPa, and the modulus is 120 GPa. Microstructure details can be found in Ref. [14]. Specimens and pads were low stress ground and polished to a RMS 8 μin. surface finish.

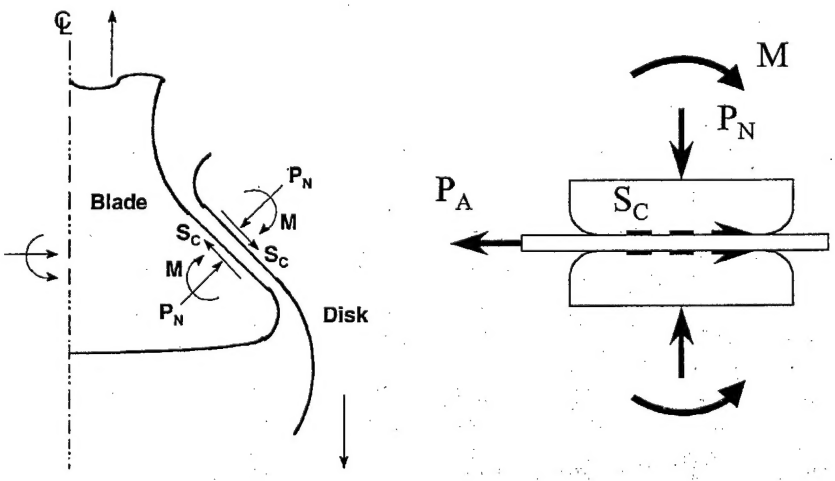

Fig. 1. Blade/disk attachment and experimental apparatus load schematic.

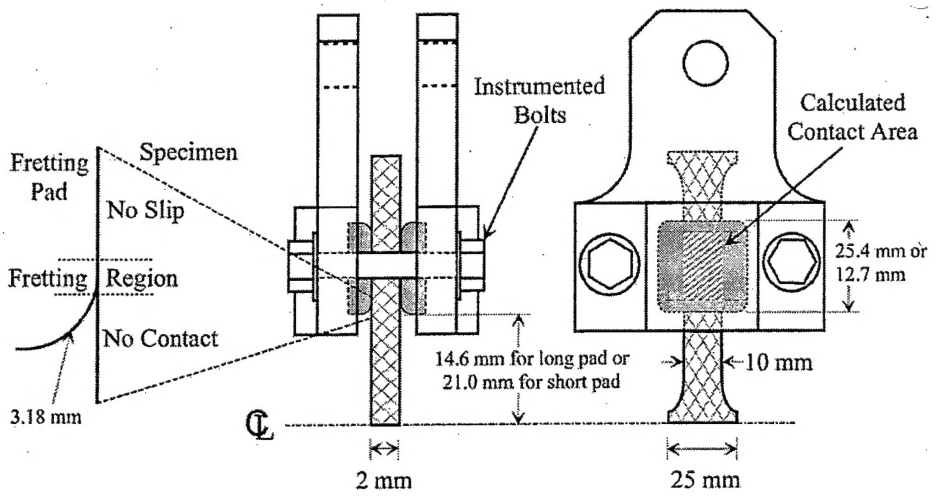

Fig. 2. Test fixture schematic indicating pad lengths, distance from center of specimen to lower edge of pad, and blending radius at EOC.

2.2. *Fretting fatigue apparatus and test conditions*

In the apparatus used for this investigation and in related investigations [11–13,15], a relatively thin, flat specimen was tested against flat pads with a specified blending radius at both edges of contact (see Fig. 2). Unlike many typical fretting fatigue test systems, the fretting pads were contained in what is usually considered the grip region, and all the load applied to the specimen was transferred to the fretting pads through shear. Hence, gross sliding is eliminated for all valid tests and damage is accumulated in a relatively small slip region that occurs at the edge of contact (EOC) (Fig. 2). In this unique configuration the fretting fatigue conditions in each grip are applied independently. For this study, nominally identical fretting fatigue conditions were applied to both ends of the specimen (Fig. 3). For specimens that were tested to fracture, one end would fail leaving the other end intact for further characterization. These were identified as '100%-of-life' tests. For specimens that were tested to some fraction of expected total life, two fretting regions were available for characterization—the region indicated by 'A' at one end of the specimen, and the region indicated by 'B' at the other end of the specimen in Fig. 3.

Two fretting fatigue conditions were selected, based on an earlier work [13]. Nominal fretting pad lengths were 12.7 and 25.4 mm. A blending radius of 3.18 mm was used, resulting in undeformed contact lengths of 6.35 and 19.05 mm. A constant average clamping stress of ~200 MPa was obtained using the longer contact length; an average clamping stress of ~620 MPa was obtained using the shorter contact length.

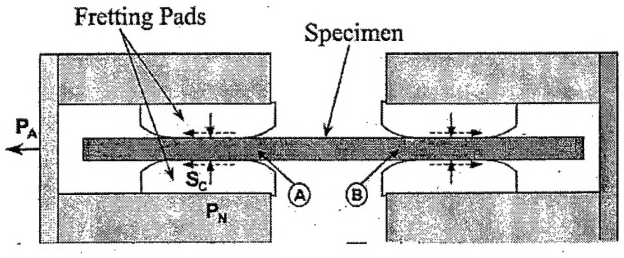

Fig. 3. Test load train schematic. Letters indicate regions of the specimen subject to fretting fatigue.

In an earlier work, the cyclic axial fretting fatigue limit stress for a 10^7 cycle fatigue life was determined to be ~350 MPa for the lower clamping stress (mean value from six tests—maximum = 405 MPa; minimum = 300 MPa) and ~250 MPa for the higher clamping stress (mean value from six tests—maximum = 276 MPa; minimum = 235 MPa) [13]. These values may be compared to the Haigh stresses, identified in third column of Tables 1 and 2 for the fretting fatigue portion of the 100%-of-life tests. Relative slip values for these two combinations of axial fatigue and clamping stress have been calculated using finite elements in prior work and are of the order of tens of microns at the EOC, with the value for the ~200 MPa clamping stress condition being higher than the value for the ~650 MPa condition [13,15]. The clamping stresses represent the approximate range of stresses calculated for the blade root region in some stages of the fan and compressor section in aircraft turbine engines. These conditions were identified for an axial stress ratio, R, of 0.5 for tests conducted at 300 Hz under ambient laboratory conditions. Control of clamping conditions was achieved with the use of instrumented bolts so the clamping load could be monitored in situ while it was being applied. Details of the test machine and the fretting fatigue fixturing can be found in Ref. [11].

A unique specimen design, shown in Fig. 4, was used to facilitate the residual fatigue strength testing. This twin dogbone specimen was designed to allow fretting fatigue damage to be applied to a specimen suitable for

Table 1
Residual fatigue strength test results for high clamping stress fretting condition

Specimen number	Fretting test conditions			Uniaxial fatigue results		
	Normal stress (MPa)	FF failure stress or Haigh stress	NF or Nfret	Stress at failure point	Nf	Failure point
01-449	638	260	1,000,000	277	10,000,000[a]	Crack; 1.2 mm
01-450	645	260	1,000,000	840	5,778,513	Blend radius
01-455[b]	651	260	1,000,000	319	10,000,000[a]	Crack; 750 μm
01-456	649	260	1,000,000	605	3,675,872	Blend radius
01-457	652	260	1,000,000	620	252,524	Crack; 200 μm
01-458[b]	643	260	1,000,000	669	10,000,000[a]	Fretting; 25 μm
02-004	616	302.2	10,000,000[a]	483	10,000,000[a]	Crack; 150 μm
02-006	632	276.3	10,000,000[a]	663	10,000,000[a]	Blend radius

[a] Fatigue limit stress reported for 10^7 cycle fatigue life—not actual applied cycles (one 100%-of-life test for this condition is not reported because the specimen was damaged during uniaxial test setup).
[b] No surface roughness measurements taken.

Table 2
Residual fatigue strength test results for low clamping stress fretting condition

Specimen number	Fretting test conditions			Uniaxial fatigue results		
	Normal stress (MPa)	FF failure stress or Haigh stress	NF or Nfret	Stress at failure point	Nf	Failure point
01-447	238	350	1,000,000	600	1,418,744	Grip
01-448	240	350	1,000,000	538	10,000,000[a]	Grip
01-451	239	350	1,000,000	840	2,903,377	Blend radius
01-452	239	350	1,000,000	557	10,000,000[a]	Gage, non-FF
01-453[b]	238	350	1,000,000	664	10,000,000[a]	Gage, non-FF
01-454	239	350	1,000,000	550	1,900,172	Gage, non-FF
01-460[b]	234	338.7	10,000,000[a]	567	10,000,000[a]	Blend radius
02-001	212	368.3	10,000,000[a]	579	10,000,000[a]	Gage, non-FF
02-002	210	403.5	10,000,000[a]	602	10,000,000[a]	Gage, non-FF

[a] Fatigue limit stress reported for 10^7 cycle fatigue life—not actual applied cycles.
[b] No surface roughness measurements taken.

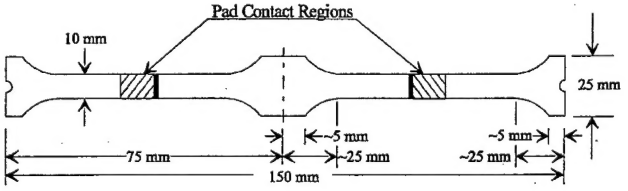

Fig. 4. Twin dogbone specimen schematic. Note: dashed line indicates bisecting line for post-fretting fatigue characterization and testing.

subsequent uniaxial testing with a minimum of post-fretting test modification. For these experiments the fretting fatigue cycles were applied to the specimen, then the specimen was bisected, as indicated by the dashed line in Fig. 4, and rectangular Ti–6Al–4V tabs of the same microstructure were laser welded to both ends to create a suitable grip section. Three fretting fatigue specimens were tested for each condition, thus producing three 100%-of-life dogbone specimens and six 10%-of-life dogbone specimens on which residual fatigue strength tests could be conducted for each clamping stress. This quantity of tests was determined to provide sufficient data from which to draw conclusions regarding trends in behavior. Width and thickness of the dogbone gage section were specified as 10 and 2 mm, respectively.

2.3. Fretting fatigue test procedures

For the 10%-of-life fretting fatigue experiments, fretting damage was applied based on the number of cycles. One million fretting cycles were applied at predetermined fretting fatigue limit stresses identified for a 10^7 cycle fatigue life for each clamping condition in the earl-

ier work [13] (see Tables 1 and 2). Then the contact was removed and the specimens were bisected to create dogbone specimens suitable for residual fatigue strength testing. The 10%-of-life damage level was selected, in part, to allow comparison of work in Refs. [2,3,16,17], where significant damage evolution up to 10%-of-life has been reported.

For the 100%-of-life tests, each specimen was tested until fracture using the same clamping conditions as those selected for the 10%-of-life tests. A step loading technique was used in applying the axial fatigue cycles, for which the specimen was loaded in fatigue at a selected load level (different from that used in the 10%-of-life tests) for 10^7 cycles. Then the stress was increased by 5% and the test was continued for another 10^7 cycles. The load steps were continued until fracture of one end of the specimen. The stress at the final block, the prior stress and the number of cycles applied at the final stress were then used to calculate a limit stress for the 10^7 cycle fatigue life, also known as a Haigh stress [18]. Failure of the specimen during the first loading block can occur, in which case the results correspond to a point on an S–N curve. Initial stress levels were selected based on the expected material fretting fatigue strength. After fracture, one dogbone section from each specimen was still intact, and bore damage accumulated at conditions nearly identical to the conditions that fractured the other end of the specimen. The fracture portion of the specimen was removed to allow characterization and uniaxial fatigue testing of the intact portion.

2.4. Characterization of fretting fatigue damage

Fretting fatigue damage was characterized using two independent techniques: scanning electron microscopy (SEM) and surface roughness measurement. Characterization in the scanning electron microscope was conducted using a small bend fixture designed to fit in the SEM chamber. By using this fixture, the specimens could be inspected in the SEM while under a small bend load that would open cracks to improve visibility. All of the imaging conducted in the SEM was done using backscatter emission that enhances variations in grain structure and elemental content. In the context of this study, the backscatter imaging augmented the wear product imaging to allow qualitative analysis of wear debris.

The second characterization technique, that of surface roughness quantification, was facilitated by a white light interferometer designed to make full field measurements of surface topography with transverse resolution of 0.1 μm and vertical resolution of 3 nm [9]. All of the scans were performed at 100× magnification. Four fretting regions (two on each side), 60μm × 45μm, were scanned on each dogbone specimen (see inset in Fig. 5). Regions along the EOC near the free edges of the specimens were selected based on optical assessments of where the worst

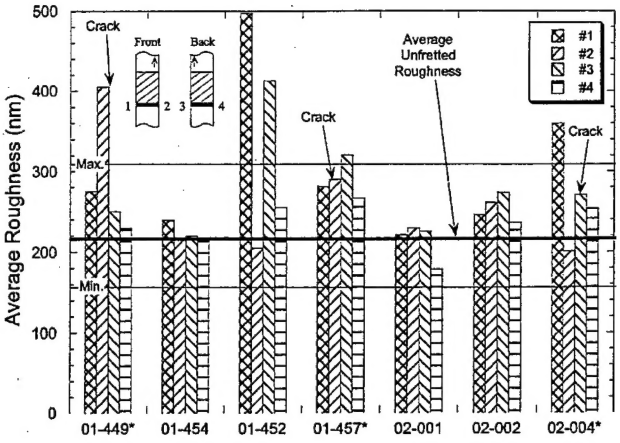

Fig. 5. Roughness results for specimens that failed in the gage section. Inset diagram indicates the scan locations that correspond to the numbers in the legend. Asterisks indicate specimens with fretting fatigue nucleated cracks.

fretting damage was located and based on results from previous work [12,19] indicating the edges as the locations most likely to nucleate fretting fatigue cracks. Details of how these locations were tracked are discussed below. Additional scans of non-fretted regions were performed to provide a baseline for comparison with the data from fretted regions. Note that surface scans to measure roughness were made in the direction of the machining texture (that is parallel to the fatigue loading axis of the specimens) to factor out machining roughness as much as possible, since the fretting induced roughnesses are of the order of the machining roughness.

The data acquisition software for the white light interferometer includes the capability to calculate average roughness values by several methods and to perform a Fourier transform of the surface profile to allow the data to be viewed in the frequency domain. By transforming the data from the spatial domain to the frequency domain, the user can view 3-D data on a 2-D plot of Power Spectral Density (PSD) vs. spatial frequency. These curves allow quantification of changes in surface roughness in a systematic fashion by quantifying the peak-to-peak asperity spacing population. The largest PSD values occur near zero spatial frequency, because the samples are nominally flat. Smaller PSD values occur for higher spatial frequencies, which correspond to closely spaced asperities. A prior investigation has indicated that the occurrence of smaller asperity spacing will increase as a function of fretting wear, thus providing a potential indicator of underlying fretting fatigue damage [9].

2.5. Residual fatigue strength tests

Following the fretting fatigue damage characterization, the dogbone specimens were heat tinted at 420 °C for 4 h in air to mark the location and size of any cracks,

and were then tested to fracture in uniaxial fatigue to quantify the remaining specimen strength. The effect of this process on crack growth behavior has been shown to be negligible [20]. As with the fretting fatigue portion of the 100%-of-life tests, these tests were completed using a step loading technique to obtain fatigue limit stresses for a 10^7 cycle fatigue life. The dogbone specimen design, which incorporates a $Kt = 1.1$, allowed quantification of residual fatigue strength reductions of 10% or more from the baseline fatigue strength of 660 MPa (for a 10^7 cycle fatigue life at $R = 0.5$) determined for this material in an earlier study [18]. Uniaxial tests were conducted at room temperature at 300 Hz and $R = 0.5$, using the same test system as that used to apply fretting fatigue cycles to retain similarity to the fretting fatigue portion of the test. In a number of cases, the estimated fatigue strength of the specimen was lower than expected. In these cases, failure occurred within the first block of the step test, and the datum became a point on an S–N curve corresponding to a life less than 10^7.

3. Results and discussion

3.1. Characterization results

The results of the characterization techniques incorporated in this study reflected changes in the surface of each specimen that might be considered fretting fatigue damage. Those changes are discussed below for surface roughness, PSD curves and SEM inspection.

Results from the surface roughness measurements are shown in Figs. 5 and 6. Fig. 5 includes roughness data for specimens that failed within the gage section. Fig. 6 includes data for specimens that failed outside the gage section. Tables 1 and 2 indicate which specimens fractured at the fretted region. Specimen numbers are given on the x-axis of each plot and correspond to the specimen numbers listed in the tables. Specimens with numbers beginning in '01' are 10%-of-life specimens; those beginning in '02' and 01–460 are 100%-of-life specimens.

A single average roughness value is shown for each of four regions that were inspected using the white light interferometer. The regions are numbered from one to four with respect to the orientation of the specimen during fretting fatigue application (see inset in Fig. 5—note that black arrow points to the top, right edge of specimen). In Figs. 5 and 6, the measurements from the fretting fatigue regions are shown with data taken from as-machined surfaces (note: horizontal lines—bold line indicates average of 12 measurements, 'Max.' line indicates maximum as-received roughness measurement, 'Min.' line indicates minimum as-received roughness measurement). Some of the measurements reflect considerable increase in surface roughness with respect to the unfretted surfaces; however, most of the roughness values are within the scatter of measurements taken from the as-received surfaces.

The data from the full field roughness profiles were also reduced by performing a Fourier transform resulting in PSD vs. spatial frequency curves. Twelve surface profiles were recorded in un-contacted regions of several samples to quantify the level of scatter in the measurement technique for the test specimens used in this investigation. The results of the unfretted scans are shown in Fig. 7, which includes the highest and lowest curves and the average curve calculated for all 12 measurements. PSD values at the higher spatial frequencies vary by about an order of magnitude. Note that the curves shown in Figs. 7–9 show only a few data points. Cubic spline curve fits were used to represent the remaining data.

Scans of fretted regions were taken near the edges of

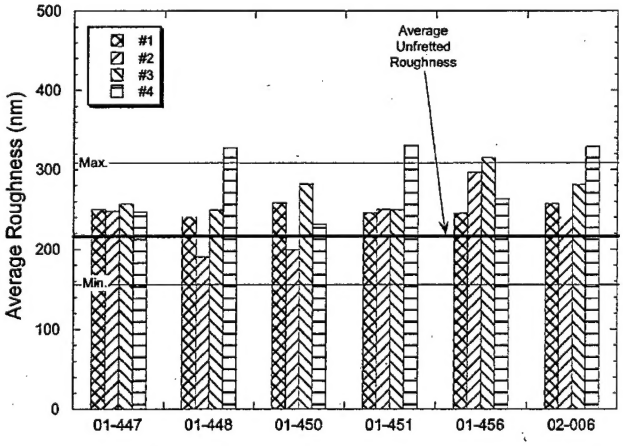

Fig. 6. Roughness results for specimens that were not tested or failed outside the gage section. See inset in Fig. 5 for definition of legend.

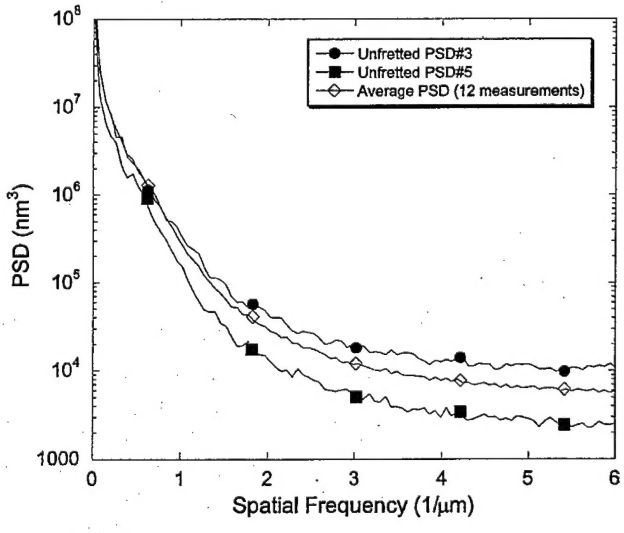

Fig. 7. Representation of scatter in roughness measurements in terms of unfretted PSD vs. spatial frequency.

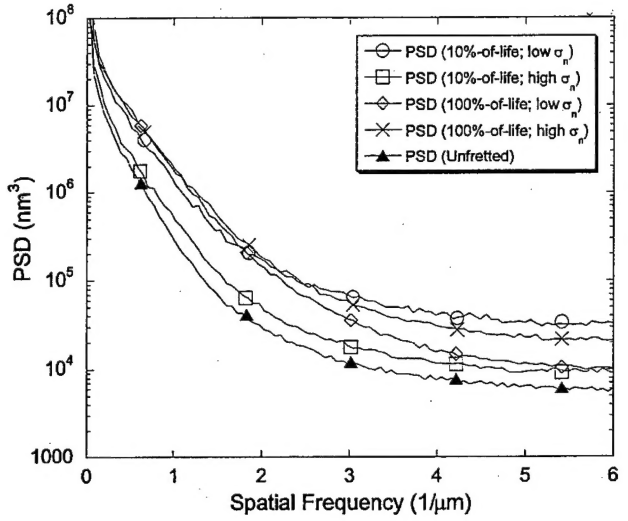

Fig. 8. Comparison of fretted and unfretted PSD data. Note: 'unfretted' data curve is the same as the 'average PSD' shown in Fig. 7.

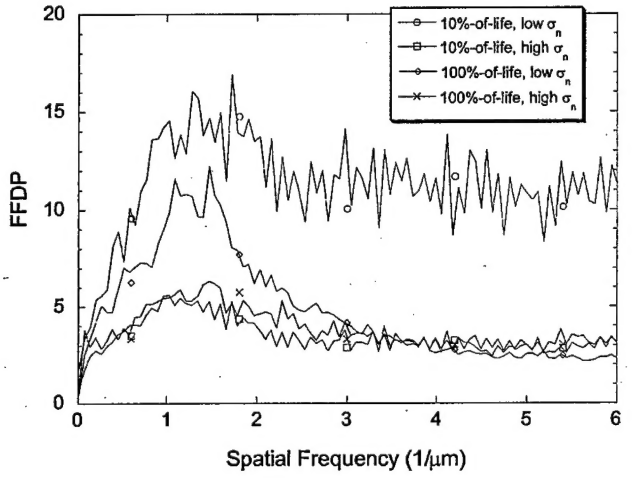

Fig. 9. Comparison of FFDP for fretted conditions shown in Fig. 8.

each specimen, where fretting fatigue cracks have been identified in previous studies [12,19] and where fretting damage appeared to be the worst. For each of these scans, the Fourier transform was performed, the PSD values were normalized with average unfretted PSD values to calculate the fretting fatigue damage parameter (FFDP) discussed below, and the PSD results were plotted against spatial frequency. The four PSD data sets from each specimen were also averaged to provide data on the general trend of damage for each specimen. Individual curves are not shown here due to space limitations. Typical average PSD curves from the four experimental conditions are shown in Fig. 8, along with the average unfretted PSD curve included in Fig. 7 (note: the hollow diamonds in Fig. 7 correspond to the solid triangles in Fig. 8). In general, a higher population of larger spatial frequency (and thus smaller asperity spacing) can be observed for all of the fretting damage levels, but particularly for the 10%-of-life+low clamping stress and the 100%-of-life+high clamping stress conditions. An increase in the population of other spatial frequencies is also present, reflecting the level of wear on the surface compared to the as-received surface.

The FFDP, which quantifies the fretted PSD deviation from the as-received condition, is shown in Fig. 9 for the same four cases shown in Fig. 8. Results for the low clamping stress condition are higher than for the high clamping stress condition. This finding is not entirely unexpected, since lower clamping stresses allow greater freedom of motion, and with greater motion comes greater wear [4,21,22]. At low clamping stress and 100%-of-life, however, the data coincide with the high clamping stress data for high spatial frequencies (>3 μm). The data for all conditions seem to peak between spatial frequency values of 1 and 2, corresponding to 1.0 and 0.5 μm asperity spacing, respectively. In the original work with this technique, the FFDP vs. spatial frequency curves were, more or less, monotonically increasing with increasing spatial frequency, but data were not recorded beyond a spatial frequency value of 1.2. Peaks, such as the ones observed here, might be expected for surfaces with initial asperity spacing of ~1.0 μm. Without considerable breakdown and embrittlement of wear debris, no particles capable of inducing smaller topographical features would be present. Such breakdown of wear debris is not typically observed under contact conditions such as these.

Each specimen was also characterized in the SEM after application of fretting damage to provide qualitative information on the level of damage generated in each test, and to identify the presence of cracks, if any. In general, wear debris was minimal, particularly for the higher clamping stress condition (see Figs. 10 and 11). None of the specimens showed sufficient wear damage to indicate a decrease in fatigue strength due to wear

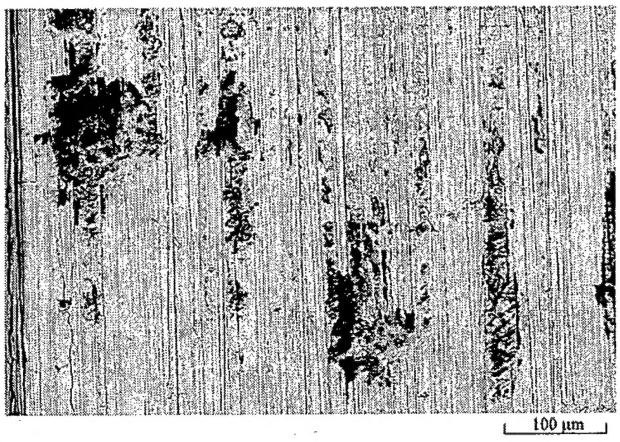

Fig. 10. Fretting damage at 10%-of-life for lower clamping stress. Average roughness ≈500 nm.

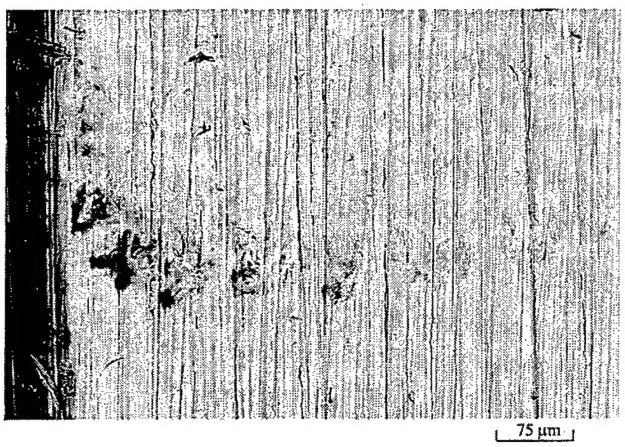

Fig. 11. Fretting damage at 10%-of-life for higher clamping stress. Average roughness ≈275 nm.

mechanisms. In some cases at the higher clamping stress, the EOC where debris usually builds up was almost indistinguishable from the as-received surface (see Fig. 11). Wear damage was worst within 1 mm of the edges of the specimens, and diminished toward the center.

Cracks were identified for approximately half of the specimens subjected to fretting fatigue under the higher clamping stress condition, indicated in Table 1. In the low clamping stress condition, however, no cracks were identified in any of the specimens on which uniaxial fatigue strength tests were to be conducted, either at the 10%-of-life or the 100%-of-life damage levels. This observation is interesting in light of findings in the literature that fretting fatigue cracks nucleate very early in life. Assuming the observations made here are an accurate representation of this particular contact condition, the findings would suggest that stress or strain criteria are a predominating factor in the nucleation of fretting fatigue cracks.

3.2. Residual fatigue strength results and correlation with characterization results

Results of the uniaxial fatigue tests are shown in Figs. 12 and 13. In Fig. 12 cycles to failure are plotted against maximum fatigue limit stress. Baseline data from earlier work on the same alloy are included for comparison [18]. Note that the cycle count for all of the data at or beyond 10^7 cycles is intended as 10^7 cycles, but some have been plotted at slightly higher cycle counts for clarity. The data from the fretted specimens are grouped by level of applied fretting fatigue damage (10% or 100%-of-life) and type of failure (fretting fatigue or non-fretting fatigue), although no apparent trend is in evidence based on these criteria. In general, the scatter in the tests that resulted in non-fretting fatigue-related failures is approximately what would be expected for fatigue lives of this magnitude. The surface length of the crack is

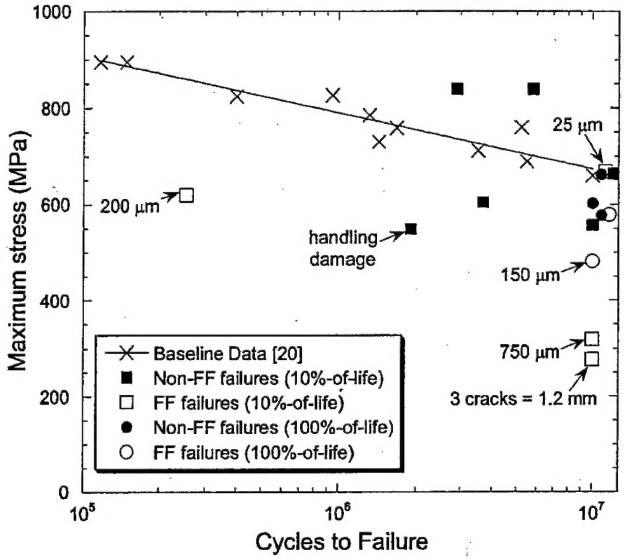

Fig. 12. Residual fatigue results for fretting fatigue damaged specimens compared with baseline fatigue results.

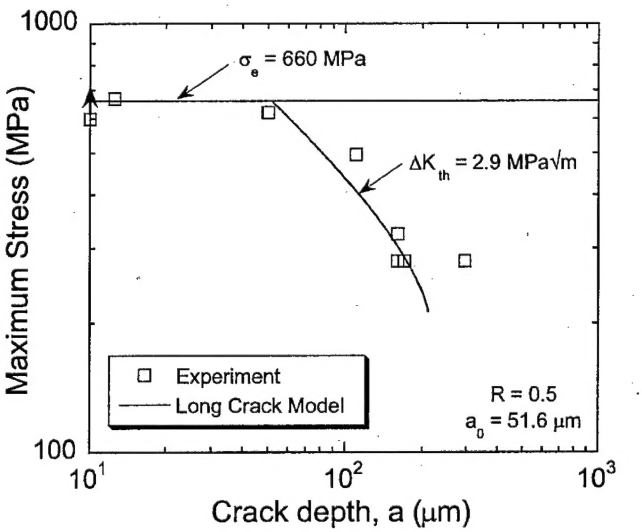

Fig. 13. Kitagawa–Takahashi type representation of residual fatigue strength results for fretting fatigue damaged specimens exhibiting cracks.

noted at the result for each specimen on which a crack was observed.

Fatigue limit stress data corresponding to 10^7 cycles from Fig. 12 are re-plotted in Fig. 13 for all specimens on which cracks were observed after fretting fatigue testing. The plot of stress as a function of crack depth, a, is in the form of a Kitagawa type diagram [23], which shows how small cracks cannot follow long crack fracture mechanics analysis because the endurance limit stress provides an upper limit for the stress corresponding to no crack. The intersection of the long crack fracture mechanics solution, corresponding to $\Delta K = 2.9\text{MPa}\sqrt{\text{m}}$, is defined as a_0. For cracks below a_0 (51.6

μm), it can be seen that there is essentially no debit in fatigue strength. In fact, for one specimen shown with an upward arrow, the fatigue failure was in a region away from the observed crack.

Of specific interest in this study is the correlation of the characterization results, discussed above, and the residual fatigue properties of each specimen. The results of each characterization technique, surface roughness, PSD vs. spatial frequency, and SEM inspection, have been described. The efficacy of each technique to quantify fretting fatigue damage will be discussed in light of the uniaxial fatigue results.

Most of the results of surface roughness measurements were determined to be within the level of scatter expected for the as-received surface, although a few were higher. As indicated in Fig. 5, higher roughness values do not always reflect the presence of cracks. Two specimens reported in the chart (01-457 and 02-004) had regions with higher roughness values than the roughness measured in the vicinity of the crack. Also, measured roughness values were very high for one specimen (01-452) on which no cracks were found. So, average surface roughness measurements do not adequately quantify fretting fatigue damage.

Asperity spacing, quantified by the PSD vs. spatial frequency curves, did not effectively identify reductions in fatigue strength either. The specimen with the highest roughness values (01-452) is represented by the curve with the hollow circles in Fig. 8. As one might expect, it also has the highest population of closely spaced asperities, but failure of this specimen occurred away from the fretting damage and at a stress consistent with the as-received material strength of ~660 MPa. On the specimen with the largest observed crack (01-449), the highest average roughness measurements occurred in the region of the crack, but the PSD vs. spatial frequency curve is only slightly higher than the average curve for unfretted measurements. It must be concluded, therefore, that for the contact geometry used in this investigation no correlation exists between surface roughness, as quantified either by asperity height (average surface roughness) or asperity spacing (PSD vs. spatial frequency), and underlying fretting fatigue damage.

The one correlation that stands out is that between crack presence, identified in the SEM, and residual fatigue strength. All but one of the specimens on which measurable cracks were identified failed at those cracks during the uniaxial fatigue tests. The size of the crack was an important factor in the remaining strength of the specimen, as might be expected (see Fig. 13). Measurable reductions in strength are indicated for specimens with cracks with surface lengths as small as 150 μm (see Figs. 12 and 13 and Table 3). However, no reduction in strength was identified for the specimen with a very small crack, 25 μm, an observation also noted in other studies for cracks nucleated under either uniaxial fatigue or fretting fatigue conditions [20,24].

After the uniaxial fatigue tests were completed, the resulting fracture surfaces were inspected, either optically or in the SEM, for all samples that fractured in the gage section. Fractography was particularly important to determine crack shape and type for the specimens determined to have fretting fatigue nucleated cracks. Fretting fatigue cracks are generally thought to be shallow compared to the surface length due to the concentration of stresses on the surface of the specimen in the vicinity of the contact. This assumption is supported by observations for the 750 μm crack (see Fig. 14) identified on 01-455. The longer crack (1.2 mm, see Fig. 15) was also shallow compared to the total surface length; however, the fracture surface revealed three smaller cracks propagating in tandem, rather than a single crack. The authors have hypothesized on the likelihood of multiple simultaneous cracks in previous work [13], but have not been able to show such irrefutable evidence before this. Aspect ratios closer to unity were observed for the smaller cracks, which might be expected considering the nature of the stress distribution. Previous work in which the stress distributions were calculated using finite elements indicated that the increases in stress generated by the presence of the clamping load on the contact tend to diminish within 100 μm or less, depending on the applied stresses [15]. Observations of the semi-elliptical crack shape for smaller cracks are consistent with the stress distributions reported in that work.

3.3. Stress intensity factors

Another important piece of information obtained from these experiments relates to the behavior of fretting fatigue nucleated cracks. It is well known that crack behavior can be affected by load history effects, and fretting fatigue cracks, which nucleate under multi-axial loading in mixed-mode in the presence of contacting components, are no exception. These load history effects include biasing the threshold stress intensity factor below which crack propagation does not take place, or $\Delta K_{threshold}$, an important factor in damage tolerant component design. Because fretting fatigue loading conditions are so complex, the exact load history of the region in which the cracks nucleate is seldom known, except in the case of Hertzian contacts where local stress distributions may be calculated.

For the experiments conducted in this study, the stress to propagate a fretting fatigue crack was effectively measured via the step loading approach used to determine the residual fatigue strength of the specimens. The $\Delta K_{threshold}$ values from specimens bearing fretting fatigue cracks were calculated from this stress and the crack size

Table 3
Stress intensity factor results calculated for fretting fatigue cracks

Specimen number	Crack type	c (μm)	a (μm)	Final stress (MPa)	ΔKa	ΔKc
01-455	Surface	350	160	324	3.9	1.9
01-457	Surface	90	50	620	3.4	2.8
02-004	Corner	125	110	496	3.5	3.3
01-449a	Surface	265	170	280	2.7	2.3
01-449b	Surface	235	160	280	2.5	2.3
01-449c	Corner	290	295	280	3.0	3.1
Baseline					2.9	2.9

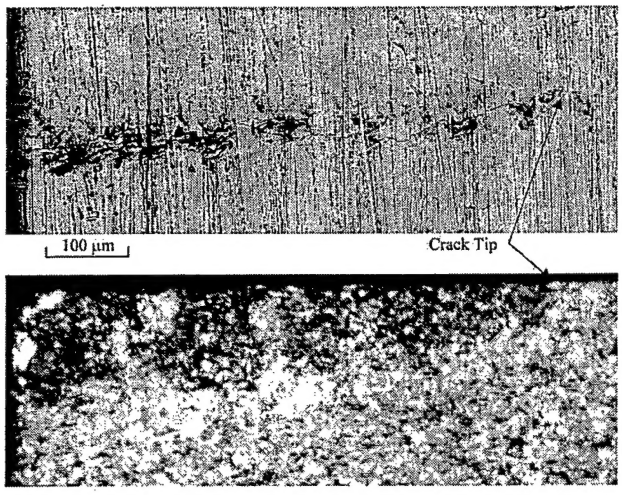

Fig. 14. SEM image of 750 μm fretting fatigue crack (above—contact region is on the top half of the image) and corresponding fracture surface (below). Specimen edge is shown to the left of the images. The dark region on the fracture surface indicates the depth of the crack at the time the contact was removed.

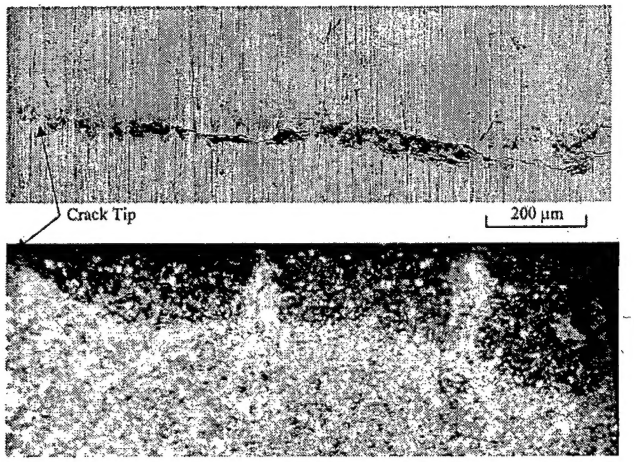

Fig. 15. SEM image of 1.2 mm fretting fatigue crack (above—contact region is on the top half of the image) and corresponding fracture surface (below). Specimen edge is shown to the right of the images. The three separate dark regions on the fracture surface indicate the size of the cracks at the time the contact was removed.

measurements taken from fracture surfaces (see Table 3 and Figs. 14 and 15).

The results for each specimen compare favorably with the $\Delta K_{threshold}$ determined for this material (~ 2.9MPa√m) for $R = 0.5$ on specimens with naturally initiated cracks that were stress relieved to remove load history effects [20]. The long, shallow crack from 01-455 seemed likely to propagate into the depth, as would be expected. The corner crack from 01-449 seemed more likely to propagate than the adjacent surface cracks, assuming no interaction between the cracks. The point corresponding to the 01-449 result on the Kitagawa diagram (Fig. 13) indicates the largest deviation from the long crack model. This result suggests that interaction between the cracks does occur and that assumptions related to crack geometry may be difficult to apply to fretting fatigue nucleated cracks. However, the authors can conclude from these results that the residual stresses expected from the fretting fatigue portion of the test did not affect resulting $\Delta K_{threshold}$ values at this stress ratio. The effect of residual stresses for lower stress ratios was not determined.

4. Conclusions

1. No correlation between surface roughness and underlying fretting fatigue damage was identified for the mixed slip–stick conditions and relative displacements of the order of tens of microns of the type produced in this test apparatus.
2. Fretting fatigue cracks having surface lengths of 100 μm or less nucleated under the conditions discussed above do not reduce the fatigue strength of the material, as shown in the Kitagawa type diagram.
3. Crack growth threshold behavior of the fretting fatigue nucleated cracks was consistent with uniaxial long crack behavior, and was not affected by any residual stresses which might develop under the conditions used in this study.

Acknowledgements

This work was performed at Air Force Research Laboratory in the Materials and Manufacturing Directorate (AFRL/MLLMN) under the National Turbine Engine High Cycle Fatigue Program and was funded under contract to the University of Dayton Research Institute, Air Force Contract No. 33615-98-C-5214. Many thanks to Dr Reji John of AFRL/MLLMN for his assistance in calculating.

References

[1] Eden EM, Rose WN, Cunningham FL. Endurance of metals. Proc Inst Mech Eng 1911;4:839–974.
[2] Waterhouse RB, Lindley TC, editors. Fretting fatigue, ESIS 18. London: Mechanical Engineering Publications; 1994. p. 219–38.
[3] Attia MH, Waterhouse RB, editors. Standardization of fretting fatigue test methods and equipment, ASTM STP 1159. West Conshohocken (PA): American Society for Testing and Materials; 1992. p. 153–69.
[4] Bryggman U, Söderberg S. Contact conditions and surface degradation mechanisms in low amplitude fretting. Wear 1988;125:39–52.
[5] Zhou ZR, Vincent L. Mixed fretting regime. Wear 1995;181-183:536–51.
[6] Ruiz C, Wang ZP, Webb PH. Techniques for the characterization of fretting fatigue damage. In: Attia MH, Waterhouse RB, editors. Standardization of fretting fatigue test methods and equipment, ASTM STP 1159. West Conshohocken (PA): American Society for Testing and Materials; 1992. p. 170–7.
[7] Fouvry S, Kapsa P, Vincent L. Quantification of fretting damage. Wear 1996;200:186–205.
[8] Murthy H, Farris TN, Slavik DC. Fretting fatigue of Ti–6Al–4V subjected to blade/disk type contacts. In: Developments in fracture mechanics for the new century, 50th Anniversary of Japan Society of Materials Science, Osaka, Japan. 2001.
[9] Shell E, Eylon D. A new method for detection and quantification of fretting fatigue damage. In: Kim NJ, Lee CS, Eylon D, editors. Light materials for transport systems 2001 (LiMAT 2001). Pohang (Korea): Center for Advanced Aerospace Materials; 2001. p. 133–40.
[10] Braun T. Veridian Engineering. Dayton, OH, unpublished work
[11] Hutson A, Nicholas T, Goodman R. Fretting fatigue of Ti–6Al–4V under flat-on-flat contact. Int J Fatigue 1999;21(7):663–70.
[12] Hutson AL, Ashbaugh NE, Nicholas T. An investigation of fretting fatigue crack nucleation life of Ti–6Al–4V under flat-on-flat contact. In: Kinyon SE, Hoeppner DH, Mutoh Y, editors. Fretting fatigue: experimental and analytical results ASTM STP 1425. West Conshohocken (PA): American Society for Testing and Materials; in press.
[13] Hutson AL. Fretting fatigue of Ti–6Al–4V under a flat-on-flat contact with blending radii. Masters thesis, University of Dayton, Dayton (OH); August 2000.
[14] Haritos GK, Nicholas T, Lanning D. Notch size effects in HCF behavior of Ti–6Al–4V. Int J Fatigue 1999;21(7):643–52.
[15] Hutson AL, Nicholas T, Olson SE, Ashbaugh NE. Effect of sample thickness on local contact behavior in a flat-on-flat fretting fatigue apparatus. Int J Fatigue 2001;23:S445–S53.
[16] Endo K, Goto H. Initiation and propagation of fretting fatigue cracks. Wear 1976;38:311–24.
[17] Nix KJ, Lindley TC. The application of fracture mechanics to fretting fatigue. Fatigue Fract Eng Mater Struct 1985;8(2):143–60.
[18] Maxwell DC, Nicholas T. A rapid method for generation of a Haigh diagram for high cycle fatigue. In: Panotin TL, Sheppard SD, editors. Fatigue and fracture mechanics, 29 vol., ASTM STP 1321. West Conshohocken (PA): American Society for Testing and Materials; 1999. p. 626–41.
[19] Hutson A, Nicholas T. Fretting fatigue behavior of Ti–6Al–4V against Ti–6Al–4V under flat-on-flat contact with blending radii. In: Hoeppner DW, Chandrasekaran V, Elliot CB, editors. Fretting fatigue: current technologies and practices, ASTM STP 1367. West Conshohocken (PA): American Society for Testing and Materials; 1999. p. 308–21.
[20] Moshier MA, Nicholas T, Hillberry BM. high cycle fatigue threshold in the presence of naturally initiated small surface cracks. In: Reuter WG, Piascik RS, editors. fatigue and fracture mechanics, 33 vol., ASTM STP 1417. West Conshohocken (PA): American Society for Testing and Materials; in press.
[21] Blanchard P, Colombie C, Pellerin V, Fayeulle S, Vincent L. Material effects in fretting wear—application to iron, titanium and aluminum alloys. Metall Trans A 1991;22:1535–44.
[22] Fouvry S, Kapsa Ph, Vincent L. Analysis of sliding behavior for fretting loadings: determination of transition criteria. Wear 1995;185:35–46.
[23] Kitagawa H, Takahashi S. Applicability of fracture mechanics to very small cracks or the cracks in the early stage. In: Proceedings of the Second International Conference on Mechanical Behaviour of Materials, Boston, MA. 1976. p. 627–31.
[24] Nicholas T. Step loading, coaxing and small crack thresholds in Ti–6Al–4V under high cycle fatigue. In: Chan KS, Liaw PK, Bellows RS, Zogas TC, Soboyejo WO, editors. Fatigue—David L Davidson Symposium. Warrendale: TMS (The Minerals, Metals & Materials Society); 2002. p. 91–106.